

Experimental Investigations of Hybrid Nanoparticles Blend Paraffin Wax [Pcm] For Enhancement of Thermal Conductivity and Heat Transfer Characteristics

^[1] M. Velliangiri , ^[2] G. Sureshkannan , ^[3] M. Karthikeyan, ^[4] K. Karthik

^{[1][3][4]} Assistant Professors Department of Mechanical Engineering, Coimbatore Institute of Technology- Tamilnadu- India

^[2] Associate Professors Department of Mechanical Engineering, Coimbatore Institute of Technology- Tamilnadu- India

Abstract: The study set out to find out the effects of experimental work and get a better understanding of the increased thermal conductivity of PCM, in this case, Paraffin Wax (PW). Experimentally concluded that using Alumina and Copper nanoparticles produced the most excellent thermal conductivity and that Alumina and Copper's nanoparticles had the most significant impact on the conductivity of PCM. Furthermore, mass fractions of prepared PW-Alumina and PW-Copper composites via sonication were 5%, 10%, and 15%, respectively. PW and composite PCMs were examined with scanning electron microscopy for their morphology (SEM). Thermophysical property testing methods were employed as the standard testing procedures. Latent heat and specific heat were measured with a differential scanning calorimeter (DSC). Heat pipe apparatus was used to conductively test thermal conductivity (which was discovered using SEM). In this study, improved thermal conductivity and latent heat were observed in composite PCMs. The enhancement ratio was 10% to 80%, at 15% total weight. Three-stage was measured using a thermocouple and piezoelectric pressure transducer, while temperature data was measured using a temperature logger. Once the experiment reached steady-state temperature, it took 35 seconds to move on to the next stage

Keywords: Alumina, Composite PCM, Copper, Mass fraction, Paraffin Wax, Phase Change Material, Thermal Conductivity

INTRODUCTION

The PCM functionality is better to work to improve the nanoparticle scattering and predict the thermal property. The phase change material (PCM) has a higher thermal conductivity when compared to the base material. Because of increased thermal conductivity and reduced latent heat from fusion, a higher NEPCM heat release rate was found than conventional PCM. The heat pipe is frequently utilized in various devices like energy storage devices and computing devices, including microprocessors, electronics, and electrical drives. PCM-heat pipes aimed at learning more about the possibility of increased efficiency, helpful materials, compatibility, and a long time ability to transport large amounts of heat in air and water. [1][2]. This research aims to select a suitable PCM multi-stage high-temperature heat pipe, which has the highest long-term heat transfer, and examine how PCM multi-stage high-temperature heat pipes predict long-term heat transfer and develop multi-stage high-performance heat pipes. In a single-stage heat pipe with a

sintered porous nickel wick structure, a 316L stainless steel material tube was selected, and the combination of an integral brazed cartridge heater and a fused sintered porous nickel wick produced a 600 to 700 °C operating temperature. In a previous research study, which explored a representative Stirling Space Power Converter heat pipe, it was found that it operated at nearly 700 °C, and that design used Inconel 718 envelopes and stainless steel screen wicks. This Haynes 230 hybrid heat pipe, which is heated by gas and passively cooled by the sun, has operated for approximately 20,000 hours and has yet to show any signs of deterioration. [7][8]. However, the previous heat pipe was unsuitable for the given design value, concerning which it was found that the heat pipe generated heat unevenly. Thus, this research paper aimed to create a suitable variable heat load, high-temperature heat pipe cascade. [10][11]. It is mandatory to select suitable materials for heat pipe, fluid property, and geometry parameters to meet the requirement. The following procedure is used to achieve maximum design: First, single- and multi-stage heat pipes like the container

are selected. Then, tubes are selected. Third, wicks are selected for working fluid. Fourth, the volume of the condenser, evaporator and evaluating the design limits are completed. [12] [13][14].

2. Design methodology and experimental setup of PCM heat Pipe

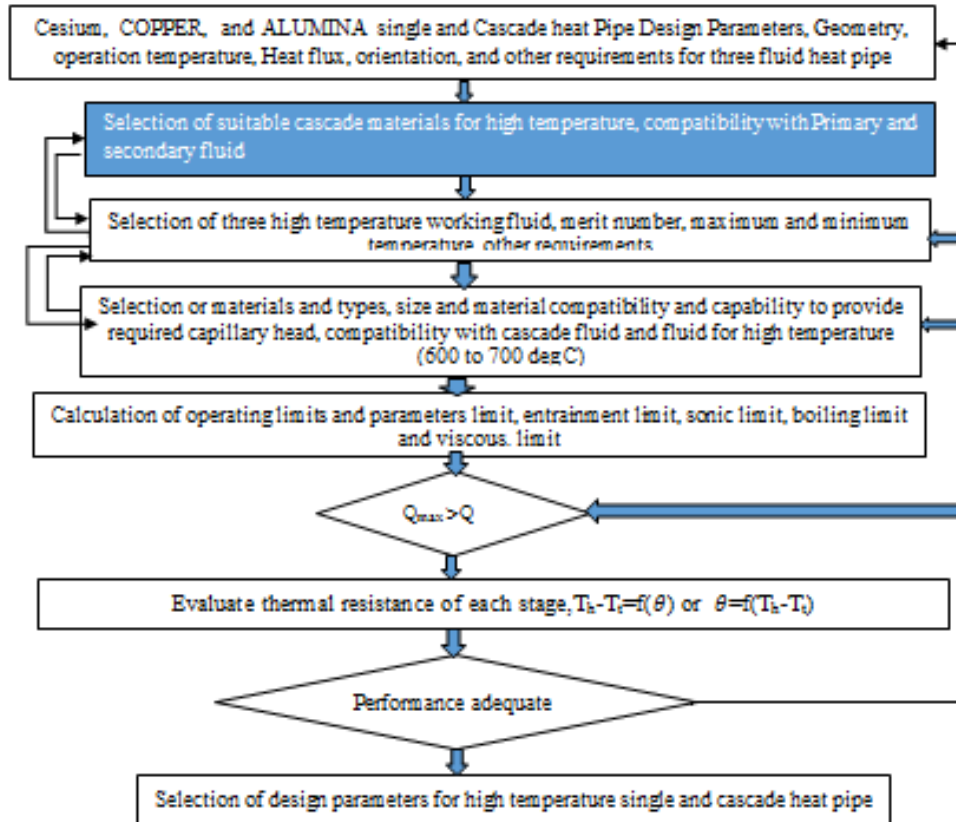


Figure: 1 Design Procedure methodology for PCM cascade high-temperature heat pipe

PCM is commonly utilized in solar research, especially when it comes to thermal storage. Research on the effects of nanoparticles of metals and nonmetals on the thermal properties of mixtures has also been conducted using PCM as a testing medium[15]. The Copper was divided into nanoparticles of paraffin wax (PW) and the PCM-Nanoparticles mixture[16]. Three samples were made: one had only paraffin wax, the other had 1% copper powder, and the third had 150% paraffin and 2% copper powder. For melting, solidifying, and thorough mixture heat analysis, a calorimeter that measures heat difference is used[17][18]. Transmission of electrons 20nm Copper Powder's form and size will be determined using microscopy. The study discovered that nanoparticles

mixed with PCM thermoelectric heat conductivity had a higher conductivity. Reduced melting point and heat flow reduce the nanomaterials to their molten state, but latent fusion heat has been amplified. In tests, paraffin wax has been shown to suspend copper powder particles whose diameter is 20 nanometers in diameter[19][20]

Figure 2.1 illustrates the application of design and parameter selection methods for single and cascade heat pipes; however, using this method to select suitable devices and procedures is ineffective[21][22]. The design procedure was followed step-by-step, and tables 1 and 2 display the properties of the fluid. Many intensive investigations in heat pipe research produced rapid commercialization and a wide range of applications[23][24]. After selecting the working fluids,

the next step was to predict the operational temperature and intended uses.[25] The operating materials and wick materials, along with the type of fluid, have been selected for excellent heat transfer. Forgiven applications and experiments, the best working fluid is chosen[26][27]. Choosing the appropriate wick for the given task is based on selecting a type that delivers the needed capability

head at the given temperature[28][29].

3.0 Selection Procedure of single and multi-stage-cascade heat pipe for PCM

The systematic procedure and equations shown in Figure 2.2 were followed to design and fabricate a temperature heat pipe.

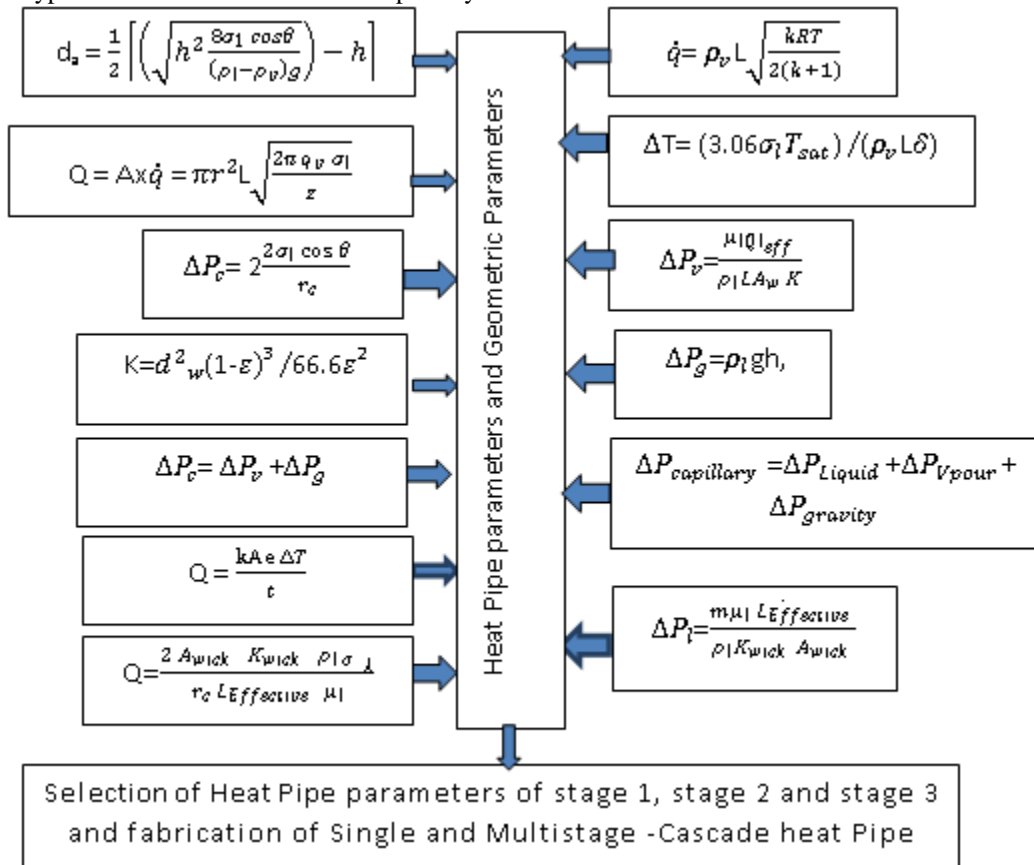


Figure 2 High temperature single and (PCM) cascade Heat Pipe Design Procedure

While PCMs have unprecedented behavioural changes, they are essential to developing many renewable energy and engineering systems in the sustainable future. PCM has become an excellent candidate for many engineering applications, including thermal, civil, electronics, and textiles. While PCMs have taken engineers to heat and excellent micro-electronic systems for modern buildings and intelligent textiles to make them more convenient today, nano-PCMs have taken them to extreme heat and lower-grade micro-electronic systems. Also, modern buildings have several built-in systems that enable the use

of heating and cooling. Nano-PCM-based energy systems are now a crucial component in helping to cut global gas emissions. This review understands various PCM types, the integration of nanomaterials, and the numerous nanomaterials' applications in PCM systems. Common types of PCM include water, paraffin, hydrated salts, and bio-based PCM. Due to their high latent thermal storage benefit, nanomaterials are incorporated despite having a low thermic effect. At a surface to volume ratio (SV/V) of more than one, nanomaterials adjust the thermal properties of the base PCM. This includes aluminium, silicon dioxide, tin oxide, carbon nanotubes (CNT),

carbon nanofibers (CNF), aluminium hydroxide, sodium hydroxide, etc.

Table 1 Operating Temperature, operating max temperature working fluid and Envelop Materials for Heat Pipe

Sl.No	Description of fluids	Boiling points, °C	Useful range, °C	Merit number W/m ²	Thermal Conductivity K (W/m-K)
1	Mercury	361	250 to 650	1.63x10 ⁹	
2	Cesium	670	450 to 900	2.1x10 ⁹	35.9
3	COPPER	774	500 to 1000	8.0x10 ⁹	100.0
4	ALUMINA	892	600 to 1200	1.8x10 ⁹	142.2
5	Lithium	1340	1000 to 1800	64087x10 ¹⁵	
6	Silver	2212	1800 to 2300		

Source: <https://www.1-act.com/merit-number-and-fluid-selection>

The materials list and the design procedure and methodology of calculations are based on some experiments and suggestions, as seen in table 1. Using design methodology, the design and materials choices are made. To understand these types of conflicts, it is essential to examine the damage to one of the parts and the different parameter setting procedures used. Properties that allow sound vapour diffusion, good vapour retention, appropriate vapour pressure, and compatibility with wick and container materials a great deal of latent heat, a high heat conductivity resistance to wetting viscosity is low, with good freezing and pour point, and vapour and liquid viscosity levels, which are also predicted. Liquid freezing and pour points are listed in Table 2. $N_l = (\sigma l L \rho) / \mu l W/m^2$, where σ, ρ, μ , and L are the surface tension, density, viscosity, and latent heat of the fluid. The merit number dimension is W/m². A heat capacity of the fluid translates to an adequate merit number [18].

The value of a merit number, which denotes the capacity needed to transport a specific thermal load, is proportional to the required sectional area. Figure 2 displays the merit number versus temperature for several heat pipe working fluids. This chart illustrates why the heat pipe working fluid is usually chosen whenever possible. For comparison, all else being equal, it is equal to 10 times as much as the liquid metal, carrying ten times as much power. A significant number of fluids serve a work function in the system. More than a dozen materials are used in the design of the wick. Selecting the right combination of material and fluid is a constant struggle. This experimental layout has heat pipes cascading to a

single point. The experimental layout is shown in Figures 2.3 and 2.4. From 4,000K to 23,000K, both single and cascade heat pipes must work within various temperature ranges. Fluid requirements also vary based on temperature. In other words, helium was used in the range of 4 Kelvin.

T1-Water inlet Temperature, T2- Heater Temperature, T3- Evaporator Temperature, T5, T7 and T8- Stage 1, 2 and 3 condenser Temperature, and T4, T6, T9- Stage1, 2 and 3 water outlet Temperature, T7- Condenser Temperature, T8- Water outlet temperature, T8- Water outlet temperature. RM-Rotameter water flows control.

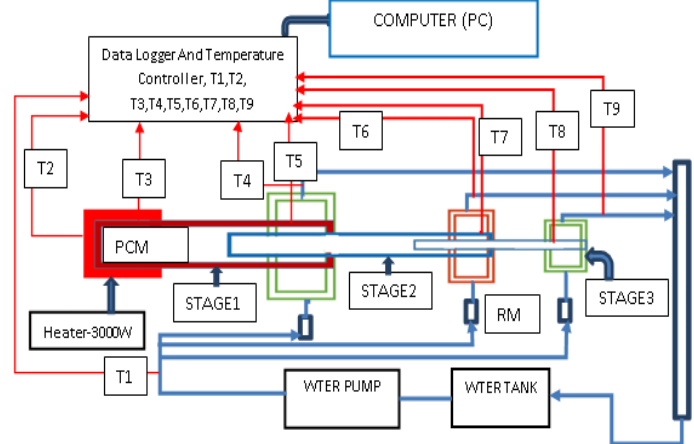


Figure 3 Experimental Layout of High-temperature PCM- cascade heat pipe

In Figure 3, the schematic diagram of the multi-stage stage heat pipe experiment setup. The experimental setup includes an evaporator and condenser; the components are

known as the experimental setup. This second heat pipe condensate is used to supply the third stage, as shown in Figure 3. The primary heat pipe stage and the second stage heat pipe are embedded in the experimental setup's first stage. A heater is used in the setup, where a stable watt is supplied to the system with a regulator. The

regulator ensures that amps are delivered. The primary reservoir's heater is located at the bottom.

Table 2 Operating Temperature, operating max temperature working fluid and Envelop Materials for Heat Pipe with Thermophysical Properties.

Authors	Nano-PCMs	Thermophysical Properties		
S. Yu et al. [11]	Bio-based PCM/xGnp (1, 3, 5wt %)	$k \sim 0.274, 0.612, 0.670$ (W/m K)	$T_m \sim 304.35, 303.75, 302.75$ (K)	$L_h \sim 146.6 \times 10^3, 144.5 \times 10^3, 143.5 \times 10^3$ (J/kg)
	Bio-based PCM/CNT (1, 3, 5wt %)	$k \sim 0.410, 0.490, 0.536$ (W/m K)	$T_m \sim 302.35, 304.45, 304.75$ (K)	$L_h \sim 133.4 \times 10^3, 132.4 \times 10^3, 130.1 \times 10^3$ (J/kg)
Shuying Wu et al. [12]	Cu/paraffin (1wt %)	$k \sim 0.2908$ (W/m K) $C_p \sim 2.924 \times 10^3$ (J/kg K) $\rho \sim 908$ (kg/m ³)	$T_m \sim 329 - 333$ (K)	$L_h \sim 183.9 \times 10^3$ (J/kg)
S. Mossaz et al. [15]	Therminol 66(t66)/NaOH KOH	$k \sim 132.2$ (W/m K) at 40 °C $\rho \sim 1077$ (kg/m ³) at 20.1 °C	---	$\mu \sim 0.136$ (Pa-s) at 20 °C
S. Harikrishnan et al. [43]	(Lauroic acid +stearic acid)/TiO ₂ (1wt %)	---	$T_m \sim 307.58$ (K) $T_f \sim 302.62$ (K)	$L_h \sim 173.22 \times 10^3$ (J/kg) $L_{hf} \sim 170.19 \times 10^3$ (J/kg)
	(Lauroic acid +stearic acid)/ZnO (1wt %)	---	$T_m \sim 307.62$ (K) $T_f \sim 302.71$ (K)	$L_h \sim 173.64 \times 10^3$ (J/kg) $L_{hf} \sim 170.57 \times 10^3$ (J/kg)
	(Lauroic acid +stearic acid)/CuO (1wt %)	---	$T_m \sim 307.71$ (K) $T_f \sim 302.77$ (K)	$L_h \sim 173.86 \times 10^3$ (J/kg) $L_{hf} \sim 170.08 \times 10^3$ (J/kg)
M. Karthikeyan et al. [58]	Nanoencapsulated paraffin	---	$T_m \sim 337.45$ (K)	$L_h \sim 74.2 \times 10^3$ (J/kg)
S. Wi et al. [59]	Coconut oil/xGnp SSPCM	$k \sim 1.3303$ (W/m K)	$T_m \sim 300.08$ (K)	$L_h \sim 82.34 \times 10^3$ (J/kg)
	Palm oil/xGnp SSPCM	$k \sim 1.2638$ (W/m K)	$T_m \sim 291.48$ (K)	$L_h \sim 77.18 \times 10^3$ (J/kg)
A. O. Elsayed [60]	(6%Al+6%Cu)/NPG	$k \sim 0.352$ (W/m K) $C_p \sim 1.786 \times 10^3$ (J/kg K) $\rho \sim 1619$ (kg/m ³)	---	$L_h \sim 74.5 \times 10^3$ (J/kg)
Zhong et al. [73]	Graphene aerogel(GA)/Octadecanoic acid PCM	$k \sim 2.635$ (W/m K)	---	$L_h \sim 181.8 \times 10^3$ (J/kg)
Ho C J et al. [74]	Octadecane emulsions/Al ₂ O ₃ (0, 5, 10wt %)	---	$T_m \sim 299.65, 299.15, 299.45$ (K) $T_f \sim 298.25, 298.15, 298.45$ (K)	$L_h \sim 243.1 \times 10^3, 225.6 \times 10^3, 212.3 \times 10^3$ (J/kg)
L. Jia et al. [75]	TiO ₂ Nanofluids	---	$T_m \sim 273.45$ (K)	$L_h \sim 0.6 \times 10^3$ (J/kg)

3.1 Experimental Setup Layout of Single and PCM- cascade heat pipe

Figures 3 and 4 present the schematic diagram of the single and PCM heat pipe experiment setup. The experimental setup includes an evaporator and condenser; the components are known as the experimental setup. The

working fluid is distilled water, and the secondary working fluid is the secondary reservoir. A 1000W heater is mounted to the bottom of the primary reservoir of area 65mm*80 mm (192.308*103 w/m²). To ensure that the heater stays in place, the reservoir is clamped onto the system using the primary clamp. The study's heat pipe was concerned with the heat transfer of two phases, and the first one dealt with a single-stage heat pipe (with

variable heat load), while the second addressed a multi-stage heat pipe (Cascade heat pipe). A single-stage heat pipe was constructed using a 1000 mm long, 30

Table 3 Operating Temperature, operating max temperature working fluid and Envelop Materials for Heat Pipe with Thermophysical Properties.

Authors	PCMs	Thermo Physical Properties of PCMs				
		Thermal conductivity "k" in (W/m K)	Density "ρ" in (kg/m ³)	Specific heat capacity "C _p " in (J/kg K)	Latent heat of fusion "L _h " in (J/kg)	Melting temp. "T _m " in (K)
A.A. Altohamy et al. [9]	Water	0.561	999.84	4.182 x10 ³	334 x 10 ³	273.15
S. Yu et al. [11]	Bio-based PCM	0.2	860	---	149.2x10 ³	301.28
Shuying Wu et al. [12]	Paraffin	0.2699	900	2.95x10 ³	205.6x10 ³	329 - 333
C.J. Ho et al. [13]	Water	0.62	997	4.17x10 ³	333x10 ³	273.15
	Microencapsulated PCM	0.31	961.4	2.13x10 ³	---	309.55
S. Mossaz et al. [15]	THERMINOL 66	117.6	1007.1	1.6269x10 ³	---	---
O. Sanusi et al. [18]	n-tricosane	0.2 (solid)	796.9	156.7x10 ³	2.2 x 10 ⁵	329.15 ± 2
X.L. Wang et al. [84]	C-L Acid material code [C0.14]	0.375 (solid)	870.8	1.853x10 ³ (solid)	100.1x10 ³	---
		0.372 (liquid)		1.891x10 ³ (liquid)		
A. Zabalegui et al. [22]	Paraffin	0.21 (solid)	900 (solid)	1888 (solid)	1.8 x10 ⁵	326
		0.12 (liquid)	780 (liquid)	2272 (liquid)		
R. Hossain et al. [23]	Liquid Cyclohexane	0.127	779	1.763x10 ³	32.557x10 ³	---
B. Rajabifar [35]	Nanoencapsulated n-octadecane PCM	0.18	815	2x10 ³	244 x 10 ³	---
A.B.S. Alqaity et al. [36]	Nanosized lauric acid PCM Particle	0.147	1007	1.76x10 ³	211x10 ³	---
R. Pakrouh et al. [38]	Paraffin RT44	0.2	780 (solid)	2x10 ³	255x10 ³	314.15 - 318.15
M. Karthikeyan et al. [58]	Nanoencapsulated paraffin	---	---	---	74.2x10 ³	337.45
S. Wi et al. [59]	Coconut oil SSPCM	0.321	---	---	110.4x10 ³	299.93
	Palm oil SSPCM	0.2891	---	---	127.3x10 ³	290.41
A.O.Elsayed [60] D.K.Benson et al. [61]	Neopentyl-glycol PCM	0.25	1046	2.76 x10 ³	131x10 ³	313.15 - 316.15
A. Castell and M.M. Farid [62]	RT 21 PCM incorporated gypsum board (PCMGB).	0.2	893	1.34x10 ³	34x10 ³	291.15 - 296.15
	Macro encapsulated SP-25 A8	0.6	1380	2.5x10 ³	180x10 ³	288.15 - 303.15
K. Nithyanandam and R. Pitchumani [63]	Li ₂ CO ₃ (35%) - Na ₂ CO ₃ (65%)	1.89	2260	1.64x10 ³	344x10 ³	778.15
	Li ₂ CO ₃ (32%); K ₂ CO ₃ (35%)- Na ₂ CO ₃ (33%)	2.02	2260	1.65x10 ³	276x10 ³	670.15

Source: file:///F:/pcm%20data/JESTR.pdf
mm diameter copper tube connected to both ends with end caps. A filling tube was also included in the kit to charge the working fluids. The screen on the inner tube was held in place with a guided setup. The removing of the non-condensable component, a vacuum pump and a

pressure of 10-4 bar were applied for four hours at 120 degrees Celsius. Then the heat pipe was cooled by placing ice cubes on top of it, and then, with the aid of a syringe, the fluid of the desired quantity (210 ml) was injected into it through a capillary tube that was calibrated to create the required vacuum (7.38 kPa).

After being crimped and sealed, the capillary tube was done. These sections of the evaporator are 100, 600, and 300 mm, respectively. The adiabatic section of the heat pipe was maintained at adiabatic conditions by using glass wool insulation and was ensured by using isothermal boundary conditions. 40x70 flat fins also increased the heat pipe fins' heat transfer capacity, each of 0.6 mm thickness mounted on the condenser section to hold the fins in place. Identical procedures were followed, and three-stage fabricated cascade heat pipe (Multi-stage) and three-stage fabricated cascade heat pipe (Multi-stage) were made, tested, and were seen in Figure 2.3. Table 1 specifies the specifications of the single and multi-stage heat pipe. In the experiment shown in Fig. 2.3, the resistance heater (of 1500W power output) is joined with a wattmeter (which displays power in watts) and an auto transfer to provide the power supply for the heater. The thermocouple readings were recorded using the Ni-based recording system used at different positions along the heat pipe. To measure the temperature response, thermocouples of K-type (10 numbers) were used. Fig. 3 illustrates the arrangement of thermocouples.

Single-stage and PCM multi-stage heat pipe. A 150-mm multi-stage heat pipe was fabricated using single-stage, adiabatic, and condenser sections, while a 300-mm version was built from three-stage, adiabatic, and condenser sections and details are provided in Table 3. For each single-stage adiabatic heat pipe, isothermal boundary conditions were maintained, and flat fins, each one of one millimetre thick, were added to augment heat transfer capacity. Preventing from flinching The cascade (multi-stage) heat pipe process was followed and was used to fabricate the heat pipe. It was tested, and the results were shown in Figure 2.2.

Table 1 presents the specification of single and multi-stage heat pipes. Fig. 2.2 is an experimental setup of a

1500W resistance heater, a wattmeter, and an auto-transfer for the heater. The NI-based thermocouple data collection system was utilized to collect data from the heat pipe at various locations. To measure the temperature response, thermocouples of K-type (10 numbers) were used. Fig. 3 illustrates the arrangement of thermocouples. To measure the inlet and outlet temperatures of the cooling water, a two-T thermocouple was used with a data logger to record the measurements. The control valve was used to measure the mass flow rating of cooling water. Glass wool, insulated with 1 cm thick, was placed on the heater and adiabatic sections, with power supplied by an autotransformer. To change the amount of heat input, and simply change the power of the variable transformer from 60 to 300 W. During steady-state operation, the mass flow rate of water was measured. We conducted three separate experiments in the same manner, using the same process, and the data is used for evaluation. The cascade heat pipe experiment involved three stages: the first contained water, ethanol, and acetone; the second contained water, ethanol, and acetone; and the third contained water, ethanol, and acetone.

4.0 RESULTS AND DISCUSSION

In calculating the variation of thermal resistance, the effect of nanoparticles on heat pipe performance can be explained. To calculate the thermal resistance of the heat pipe, one must first find the temperature difference between the evaporator and condenser walls, which is also called the "thermal differential". Table 3 provides thermal resistance expressions for various sections of the heat pipe.

The variation of thermal resistance of the heat pipe filled with and the copper nano-particles suspension are presenting in Fig. 4.

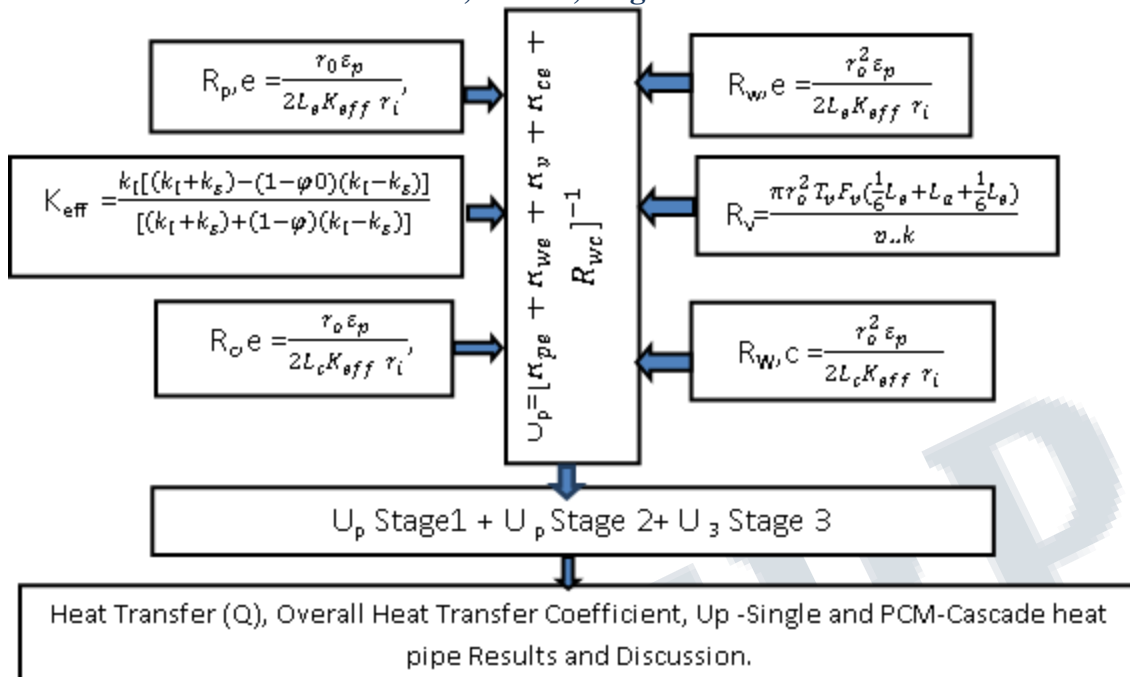


Figure 4. Overall heat Transfer Coefficient calculation procedure for single and multi-stage (PCM-cascade system) heat Pipe.

The overall trend for thermal resistance suggests that the overall heat input results in a decrease in the heat pipe's thermal resistance. The thermal resistance was reduced by 32.10% in response to using 0.01% of copper nanoparticles. The experimental results show that heat input using the nanofluid in the heat pipe results in lower thermal resistance. By activating many nucleation sites in the evaporator section, extending the nucleate boiling regime, the reduction in thermal resistance is obtained.

Single and PCM multi-stage heat pipe: Error estimation of single and PCM-stage heat pipe Error estimates are essential for experimental results and analyses, and they influence them. Additional experimental sources of uncertainty included coolant flow rate and wattmeter measurements. The error analysis for flow measurement was completed and tabulated, resulting in an estimated flow measurement accuracy between +2.5% and -2.5%. The estimated accuracy of the thermocouple is around 5%. According to Holman, the maximum uncertainty in the wattmeter is ±1.5 w., and the error analysis is concluded with the following method. In addition to the heat flux and transfer coefficient uncertainties predicted and tabulated in Table 3, the other uncertainties were calculated using equations 1 and 2.

$$q_c = \sqrt{\left(\frac{\partial q}{\partial Q} w_Q\right)^2 + \left(\frac{\partial q}{\partial D} w_D\right)^2 + \left(\frac{\partial q}{\partial L_c} w_{L_c}\right)^2} \quad (4)$$

$$h_c = \sqrt{\left(\frac{\partial h_c}{\partial q_c} w_{q_c}\right)^2 + \left(\frac{\partial h_c}{\partial \Delta T} w_{\Delta T}\right)^2} \quad (5)$$

In conclusion, the uncertainties were found to be between 5 and 6 percent.

Symbols: W Q, W D, W (LC), W (Q C), and W ΔT In the heat flow rate, diameter, condenser length, and temperature drops, the uncertainties include these three elements.

Table 3: Uncertainty of Heat Flux and Heat transfer coefficient of single-stage and PCM- cascade heat pipe.

	Heat pipe with water		PCM-Cascade heat pipe	
Heat input	Uncertainty of Heat Flux single stage (%)	Uncertainty of heat transfer coefficient single stage (%)	Uncertainty of Heat Flux cascade system (%)	Uncertainty of heat transfer coefficient cascade system (%)
1000	6.1	6.3	6.23	6.52
1500	6.01	6.12	6.33	6.4
2000	5.33	5.11	6.04	6.3
250	5.8	5.86	6.06	6.25

0				
275	5.92	6.03	6.25	6.31
0				

output of a single-stage process was estimated using the formula.

4.2. Over all Heat Transfer Coefficient of Single and PCM -multistage

The heat transfer coefficient from Figure 2.4 was calculated as described above. $U_p = \left[\frac{1}{R_{pe} + R_{we} + R_v + R_{ce} + R_{wc}} \right]^{-1}$ (6)

The heat pipe was examined to evaluate its heat transfer capacity alongside the base fluid for single-stage and multi-stage heat pipes. Q_c is the experimental heat transfer coefficient, Q is the heat transfer rate, and l_c is the condenser length. The total mass of water flow (m) is equal to the specific heat of water (ΔT). In order to find a cascade system, the same procedure was used. The heat

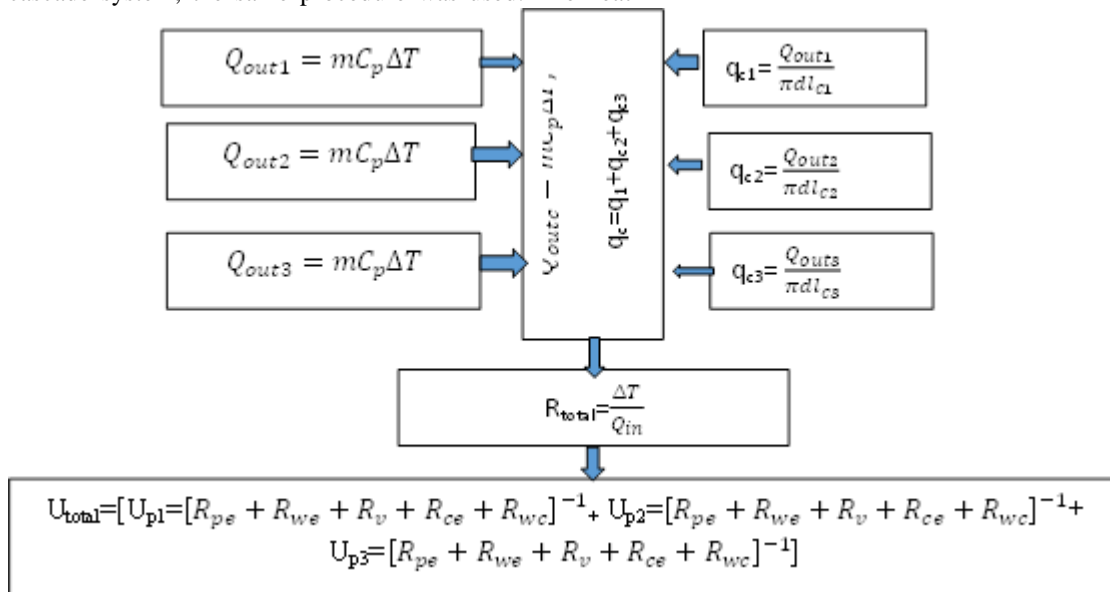


Figure 5 Heat Transfer, heat flux and Overall Heat Transfer Coefficient calculation procedure of PCM heat pipe

The figure shows the condensing heat transfer coefficient enhancement due to the addition of two stages (multi-stage) with two different fluids like ethanol and acetone. The results showed that the heat transfer coefficient of the heat pipe changed with multi-stage and compared to a single-stage heat pipe. It is believed that the heat transfer enhancement in the evaporator and condenser section is mainly dependent on the nature of the surface created by the multi-stage as the convection area was increased. The heat transfer coefficient in the condenser section depends on the thickness of the liquid

layer and the hydrodynamic properties of the working fluid. A correlation can be established between the Nusselt number, Reynolds number and Prandtl number

$$N_u = \frac{(hC_l)}{K} = 1.12Re^{0.8} Pr^{0.7} \tag{9}$$

The correlation of Eq. 9 may be compared with the existing correlation for condensing water vapour in thermosiphon as a function of Reynolds number.

$$N_u = 5.03Re^{1/3} Pr^{1/3} \tag{10}$$

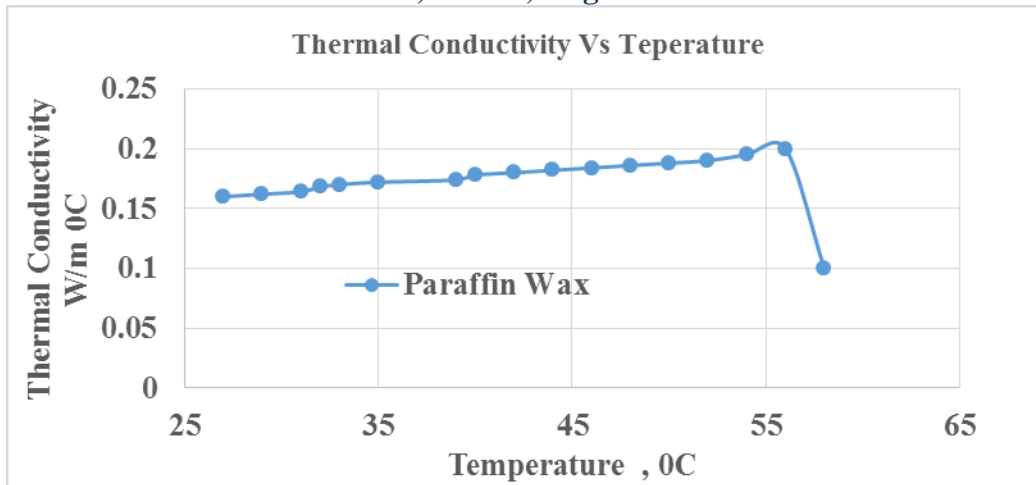


Figure 6 Temperature Vs Thermal Conductivity of Paraffin Wax PCM-multistage heat Pipe

Figure 6 shows the variation of thermal conductivity of paraffin wax shows that temperature increases with the increase the thermal conductivity up to 55 ° C and suddenly decreased.

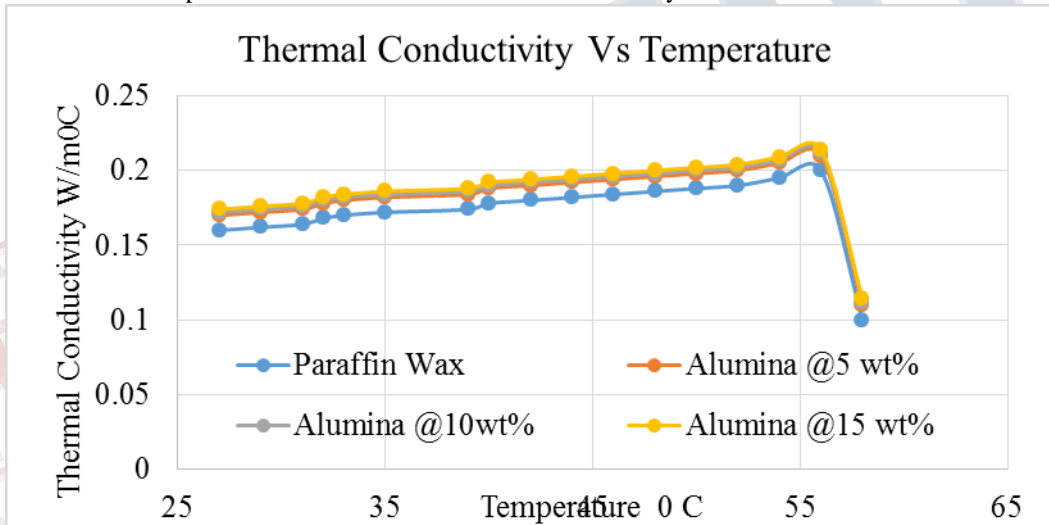


Figure 7 the variation of Thermal Resistance concerning Heat Input

Figure 7 shows the variation of thermal conductivity of paraffin wax and compares to Alumina shows that temperature increases with the increase in thermal conductivity up to 55 ° C and suddenly decreased. The trend shows an enhancement with the increase in t

thermal conductivity. Prandtl number and Reynolds number mean that the increase in the Prandtl number leads to the enhancement of the Nusselt number. The figure shows a comparison of the experimental results of the heat pipe.

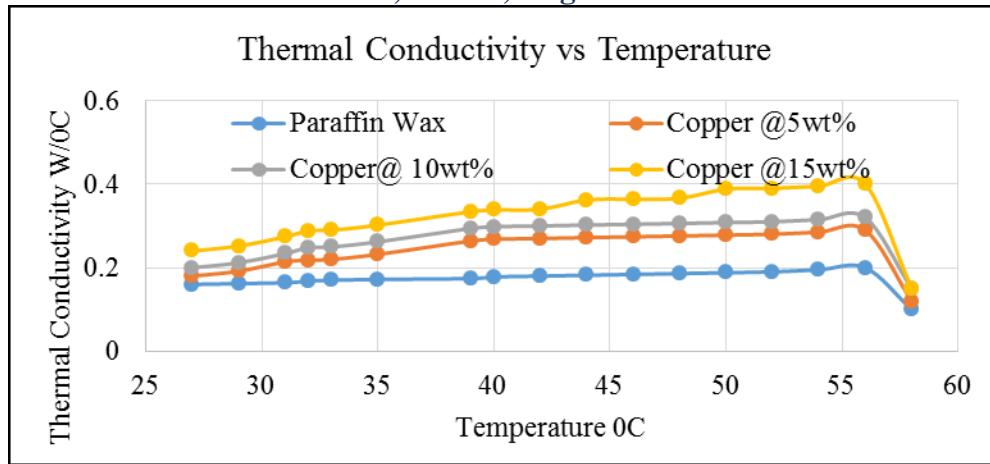


Figure 8 the variation of Thermal Resistance concerning Heat Input

Figure 8 shows the variation of thermal conductivity of paraffin wax and compares to Copper nano Particle shows

that temperature increases with the increase in thermal conductivity up to 55 °C and suddenly decreased.

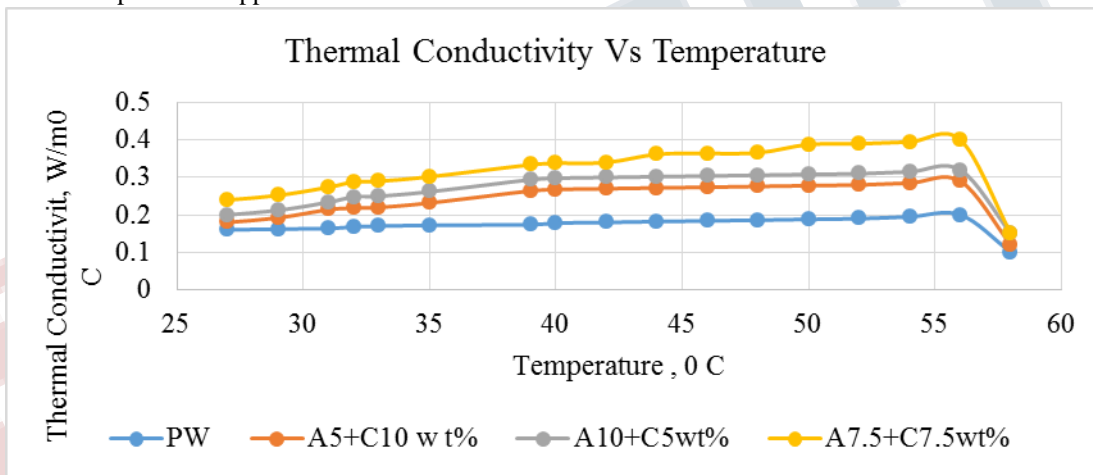


Figure 9 variation of Efficiency with Heat Input of PCM-Heat Pipe

Figure 9 shows the variation of thermal conductivity of paraffin wax and compares it to Copper nano Particle, and Copper nanoparticle shows that temperature increases with the increase in thermal conductivity up to 55 °C and suddenly decreased. When looking at the graph in Figure 9, it can be deduced that the variation of heat transfer coefficient with T_{sat} (K) shows. The increasing temperature usually increases the heat transfer coefficient. The heat pipe transfer coefficient for cascade heat pipes is about 18 to 19.5% higher than for single-stage heat pipes. Experiments were run to explore the system to learn more about the heat transfer and characteristics in the evaporator and condenser sections of the heat pipe. Condenser heat transfer depends on the Reynolds number and Prandtl number. As fluid velocity and condensate, liquid play an essential role in heat transfer; variations in heat transfer coefficient are directly related to the types of

heat pipes used. In order to understand the heat transfer characteristics of the evaporator and condenser section of the heat pipe shown in Figure 4, several single- and multi-stage heat pipe experiments were performed. When heat flux increases from 8 kW/m² to 68 kW/m², the heat transfer coefficient increases. With an increase in heat flux or the saturation temperature maximum of 23.10%, the overall heat transfer coefficient of the system increases gradually, and the heat transfer coefficient increases by 16% compared to single-stage systems

5.0 CONCLUSION

In order to understand the heat transfer properties of the single and multi-stage heat pipe, the experiment was run. Three fluids with variable heat input were simulated regarding thermal resistance and efficiency for single and

multi-stage stages. Aluminium oxide has a slightly lower thermal conductivity than Copper, and Cesium has a lower thermal conductivity and boiling point than aluminium oxide and Copper, but the boiling point was higher. Alumina had lower merit numbers than the other two fluids. The efficiency of the PCM heat pipe cascade was better than that of a single-stage cascade that operated in a range of 600 to 750 degrees Celsius. The 8% difference in single-stage heat pipe heat transfer vs cascade heat pipe heat transfer is caused by two fluids with different boiling points in the second and third stages. The amount of heat transfer increased from the experimental research because of the increased convection area in the cascade. In this study, improved thermal conductivity and latent heat were observed in composite PCMs. The enhancement ratio was 10% to 80%, at 15% total weight. Three-stage was measured using a thermocouple and piezoelectric pressure transducer, while temperature data was measured using a temperature logger. Once the experiment reached steady-state temperature, it took 35 seconds to move on to the next stage.

Nomenclature

G	- Acceleration due to gravity,
∞	- Ambient
A_{vg}	- Average
H	- Heat Transfer Co Efficient
B	- Bottom wall
T_m	- Bulk mean temperature
B	- Co-efficient of volumetric expansion,
Q_{sides}	- Convective heat loss
Q_{top}	- Convective heat loss
T_{max}	- Dimensionless temperature,
exp	- Experimental
FN	- Figure of Merit,
f	- Fluid
Gr	- Grashof number,
q_{pri}	- Grashof number,
q_{sec}	- Heat,
q''	- Heat flux (W/m^2)
Q_{in}	- Heat input, W
T_{heater}	- Heater temperature, °C
T_{water}	- Water temperature, °C
ν	- Kinematic viscosity, m^2/s
N	- Number of secondary tubes arranged

Nu	- Nusselt number, hL/k , hd/k
Pr	- Prandtl number, ν/α
pri	- Primary coolant
Ra	- Rayleigh number,
sec	- Secondary coolant
A_h	- Surface area of the heater, m^2

ACKNOWLEDGEMENT

I wish to record my deep sense of gratitude and profound thanks to my research supervisor, **Dr A. S. Krishnan.**, Associate Professor and **Dr K. Marimuthu.**, Professor, Head of the Department of Mechanical Engineering, **Dr V Selladurai.**, Principal, Coimbatore Institute of Technology, Coimbatore-641014, for his keen interest in timely motivation, inspiring guidance and constant encouragement with my work during all stages, to complete the research successfully.

Reference

- [1] G. Hansen, E. Næss, and K. Kristjansson, "Analysis of a vertical flat heat pipe using COPPER working fluid and a wick of compressed nickel foam," *Energies*, vol. 9, no. 3, pp. 1–17, 2016.
- [2] D. A. Odden, "Development of heat pipes with COPPER as working fluid: Performance limitations and test rig development," no. June 2012.
- [3] J. H. Boo, S. M. Kim, and Y. H. Kang, "An Experimental Study on an ALUMINA Loop-type Heat Pipe for Thermal Transport from a High-temperature Solar Receiver," *Energy Procedia*, vol. 69, no. May 2015, pp. 608–617, 2015.
- [4] S. W. Kang, H. M. Yeh, M. C. Tsai, and H. H. Wu, "Manufacture and test of a high-temperature heat pipe," *J. Appl. Sci. Eng.*, vol. 22, no. 3, pp. 493–499, 2019.
- [5] J. H. Rosenfeld, "An Overview of Long Duration ALUMINA Heat Pipe Tests," no. March 2004, pp. 140–147, 2004.
- [6] U. Sharma, "A Study of High-Temperature Heat Pipes and the Impact of Magnetic Field on the Flow of Liquid Metal," p. 117, 2017.
- [7] R. Materials, D. Hanna, R. Equipment, and H. Circuit, "Cesium Heatpipe Experiment," 1977.
- [8] P. M. Dussinger and W. G. Anderson, "Design

and Testing of Titanium / Cesium and Titanium / COPPER Heat Pipes,” no. September 2015.

[9] S. Lips, V. Sartre, F. Lefevre, S. Khandekar, and J. Bonjour, “Overview of Heat Pipe Studies During the Period 2010-2015,” *Interfacial Phenom. Heat Transf.*, vol. 4, no. 1, pp. 33–53, 2016.

[10] R. Andrzejczyk, “Experimental investigation of the thermal performance of a wickless heat pipe operating with different fluids: Water, ethanol, and SES36. Analysis of influences of instability processes at working operation parameters,” *Energies*, vol. 12, no. 1, 2019.

[11] Y. Fukuzawa and Y. Fujii-E, “Performance Characteristics of COPPER Heat Pipe Loaded with Argon,” *J. Nucl. Sci. Technol.*, vol. 15, no. 2, pp. 109–119, 1978.

[12] M. Narcy, S. Lips, and V. Sartre, “Experimental investigation of a confined flat two-phase thermosyphon for electronics cooling,” *Exp. Therm. Fluid Sci.*, vol. 96, pp. 516–529, 2018.

[13] P. K. Jain, “Influence of Different Parameters on Heat Pipe Performance Sharmishtha Singh Hada under the guidance of Prof,” *J. Eng. Res. Appl. www.ijera.com*, vol. 5, no. 10, pp. 93–98, 2015.

[14] M. A. Boda, T. B. Shaikh, and S. N. Sayyed, “Innovative Developments and Heat,” vol. 3, no. 6, pp. 319–322, 2018.

[15] P. Z. Shi, K. M. Chua, S. C. K. Wong, and Y. M. Tan, “Design and performance optimization of miniature heat pipes in LTCC,” *J. Phys. Conf. Ser.*, vol. 34, no. 1, pp. 142–147, 2006.

[16] A. . Chaudhari, M. D. Borkar, A. Deshpande, M. V. Tendolkar, and V. K. Singh, “Effect of Wick Microstructures on Heat Pipe Performance A Review,” *SSRN Electron. J.*, pp. 1–8, 2018.

[17] J. V. Suresh, P. Bhramara, and S. S. Krishna, “Effect of Working Fluid on Thermal Performance of Closed Loop Pulsating Heat Pipe,” *Int. J. Eng. Adv. Technol.*, vol. 9, no. 2, pp. 953–956, 2019.

[18] C. E. Andraka, T. A. Moss, V. Baturkin, V. Zaripov, and O. Nishchyk, “High-performance felt-metal-wick heat pipe for solar receivers,” *AIP Conf. Proc.*, vol. 1734, 2016.

[19] J. Jose and R. Baby, “Recent advances in loop heat pipes: A review,” *IOP Conf. Ser. Mater. Sci. Eng.*, vol. 396, no. 1, 2018.

[20] H. Masuda, A. Ebata, K. Teramae, N.

Hishinuma, Alteration of thermal conductivity and viscosity of liquid by dispersing ultra-fine particles, *Netsu Bussei* 7 (4) (1993) 227–233. Fig. 5. The instantaneous volume of the nanofluid within the square cavity. 542 J.M. Khodadadi, S.F. Hosseinizadeh / *International Communications in Heat and Mass Transfer* 34 (2007) 534–543

[22] U.-S. Choi, Enhancing thermal conductivity of fluids with nanoparticles, in *Developments and Application of Non-Newtonian Flows*, ASME, FED-Vol. 231/MD-Vol. 66, 1995, pp. 99–105.

[23] K. Khanafer, K. Vafai, M. Lightstone, Buoyancy-driven heat transfer enhancement in a two-dimensional enclosure utilizing nanofluids, *Int. J. Heat Mass Transfer* 46 (19) (2003) 3639–3653.

[24] N. Wakao, S. Kaguei, *Heat and Mass Transfer in Packed Beds*, Gordon and Breach Science Publishers, New York, 1982, pp. 175–205.

[25] FLUENT 6.1 User's Guide, Fluent, Inc., Lebanon, NH, 2003. [6] V.R. Voller, C. Prakash, A fixed-grid numerical modelling methodology for convection-diffusion mushy region phase-change problems, *Int. J. Heat Mass Transfer* 30 (8) (1987) 1709–1719.

[27] J.M. Khodadadi, Y. Zhang, Effects of buoyancy-driven convection on melting within spherical containers, *Int. J. Heat Mass Transfer* 44 (8) (2001) 1605–1618.

[28] A.D. Brent, V.R. Voller, K.J. Reid, Enthalpy-porosity technique for modelling convection-diffusion phase change: application to the melting of a pure metal, *Numer. Heat Transf.* 13 (3) (1988) 297–318.

[29] C. Gau, R. Viskanta, Melting and solidification of pure metal on a vertical wall, *J. Heat Transfer* 108 (1) (1986) 174–181. [10] J. Banaszek, Y. Jaluria, T.A. Kowalewski, M. Rebow, Semi-implicit FEM analysis of natural convection in freezing water, *Numer. Heat Transf. A* 36 (5) (1999) 449–472.